



Caustic effects on high-order harmonic generation in grapheneFulong Dong ¹, Qinzhi Xia,² and Jie Liu ^{1,*}¹Graduate School, China Academy of Engineering Physics, Beijing 100193, China²Institute of Applied Physics and Computational Mathematics, Beijing 100088, China

(Received 24 July 2023; accepted 28 March 2024; published 10 April 2024)

We employ two-band density-matrix equations and time-dependent density-functional theory to calculate high-order harmonic generation (HHG) in graphene under femtosecond laser irradiation. Our investigation uncovers a striking harmonic enhancement structure (HES) in the HHG spectrum. We find that the HES is associated with the bunching of multiple interband electron-hole recombination trajectories, in analogy to the focusing behavior of the light rays known as caustics. In contrast to the atom situation, where the caustic effects are confined to a narrow energy regime around the HHG cutoff energy, for graphene, the caustic effects can dominate the entire interband harmonic generation regime. The magnitude of enhancement is significant and can be estimated to be on the order of $\sim N^{2/3}$, with N representing the harmonic order, according to catastrophe theory.

DOI: [10.1103/PhysRevA.109.L041102](https://doi.org/10.1103/PhysRevA.109.L041102)

Introduction. The propagation of light can exhibit interesting behavior termed as a caustic phenomenon, in which multiple light rays converge and give rise to bright focusing features [1–3]. In analogy to light propagation, generalized caustic effects occur when multiple particle trajectories converge, resulting in a caustic singularity and the subsequent enhancement of physical phenomena [4–9]. The magnitude of enhancement can be approximately predicted by catastrophe theory, which associates each caustic singularity with a specific topological type of catastrophe [3]. Caustic phenomena have been observed in diverse fields, including acoustics [10], radio propagation [11], as well as high-order harmonic generation (HHG) [12–15].

Attosecond pulses [16] have sparked considerable research interest in HHG across various media, including gases [17–21], crystalline solids [22–26], and two-dimensional (2D) materials [27–31]. When an atom is irradiated by a femtosecond laser, caustic effects occur at the cutoff energy of HHG. At this critical point, two branches of electron trajectories, commonly referred to as “short” and “long” trajectories, converge and contribute to the same harmonic energy, resulting in an enhancement in the spectrum magnitude [12,32]. Recently, the discussions of caustic effects on HHG are extended to solid material such as MgO [14]. It was claimed that the Van Hove singularities in the energy-band structure might result in caustic singularity. However, the enhanced HHG spectra observed in the experiment apparently deviate from the locations of the Van Hove singularities [14]. On the other hand, theoretical investigations of the caustic effects on the HHG of a one-dimensional (1D) periodic potential model have been made [15]. Similar to atomic scenarios, it is found that caustic enhancement emerges only at a cutoff regime determined by the maximum electron-hole recombination energy [15].

In this Letter, we present the theoretical exploration of caustic effects in the HHG of the celebrated 2D material, graphene. Graphene features a periodic hexagonal lattice with two carbon atoms per unit cell and shows many interesting phenomena in the external fields [33–36]. We attempt to investigate the caustic effects of the HHG in graphene irradiated by a linearly polarized midinfrared (MIR) laser. In contrast to the atom scenario, we find that caustic effects might dominate the entire interband harmonic generation regime. In particular, the location of the HHG enhancement peak is found to correspond to the zero determinant of the Hessian matrix of the semiclassical action of the electron-hole recombination trajectories and has nothing to do with the Van Hove energy-band singularities.

Harmonic enhancement structure (HES). We perform calculations of HHG using the two-band density-matrix equations (TBDMEs) as well as the time-dependent density-functional theory (TDDFT). Here, the vector potential of the MIR laser field is $\mathbf{A}(t) = A_0 \sin^2(\omega_0 t/2n) \sin(\omega_0 t) \mathbf{e}$, where $n = 3$, and A_0 denotes the amplitude. The frequency of the MIR laser field, denoted as ω_0 , corresponds to a wavelength of $\lambda = 5500$ nm. The unit vector \mathbf{e} indicates the direction along the Γ - M axis of graphene. Throughout this Letter, atomic units are employed unless otherwise specified. The harmonic spectra shown in Fig. 1 are simulated for a laser intensity of 8×10^{11} W/cm². Both spectra exhibit a region of enhanced intensity, termed as the harmonic enhancement structure (HES) in the following (see the region marked by the blue dashed rectangle). For comparison, the Van Hove singularities (M and Γ points of graphene) are indicated in Fig. 1 as vertical dotted lines. We find that the energy of the observed HES does not match the energies of the Van Hove singularities, similar to the observations in Ref. [14].

Electron-hole recombination trajectory. To unveil the underlying mechanisms behind the HES in graphene, we investigate the electron-hole recombination trajectories in the

*jliu@gscaep.ac.cn

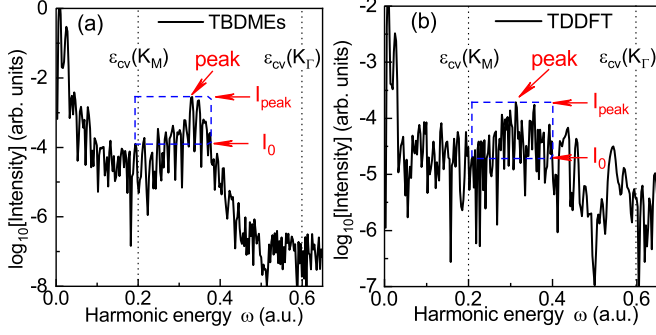


FIG. 1. The harmonic spectra calculated by (a) TBDMEs and (b) TDDFT with a laser intensity of 8×10^{11} W/cm² and a wavelength of 5500 nm. In (a) and (b), the obvious HES are marked by blue dashed rectangles, and the HES peak corresponding to the local harmonic maximum intensity is indicated by red arrows at $\omega^* = 0.34$ in (a) and $\omega^* = 0.31$ in (b). The upper and lower boundaries of the blue dashed rectangle marked by I_{peak} and I_0 correspond to the harmonic energy of the HES peak and the background harmonic energy away from the HES, respectively. The vertical dotted lines label the energy difference between the c and v bands at the Van Hove singularities (M and Γ points of graphene).

framework of TBDMEs [37]. Within the strong-field approximation formulation [38,39], the intraband currents become negligible and the interband currents play a dominant role in the harmonic generation. The Fourier transform of the total current can be expressed as

$$j(\omega) \sim \int_{\text{BZ}} d\mathbf{K}_{0x} \int_{\text{BZ}} d\mathbf{K}_{0y} \int_{-\infty}^{\infty} dt \int_{-\infty}^t dt' g(\mathbf{K}_{0x}, \mathbf{K}_{0y}, t, t') \times e^{-iS(\mathbf{K}_{0x}, \mathbf{K}_{0y}, t, t', \omega)} + \text{c.c.}, \quad (1)$$

where $\mathbf{K}_0 = (\mathbf{K}_{0x}, \mathbf{K}_{0y})$ represents the lattice momentum within the first Brillouin zone (BZ). $S(\mathbf{K}_{0x}, \mathbf{K}_{0y}, t, t', \omega) = \int_{t'}^t \varepsilon_{cv}(\mathbf{K}_x(\tau), \mathbf{K}_{0y}) d\tau - \omega t$ denotes the semiclassical action, with $\mathbf{K}_x(t) = \mathbf{K}_{0x} + A(t)$. The term $\varepsilon_{cv}(\mathbf{k})$ represents the energy difference between the c and v bands for the lattice momentum \mathbf{k} . $g(\mathbf{K}_{0x}, \mathbf{K}_{0y}, t', t)$ constitutes a slowly varying prefactor [37].

In contrast to other solid materials such as MgO and ZnO [14,39], graphene is unique, due to Dirac cones. Consequently, when employing the stationary phase approximation for all four integral variables in Eq. (1), a constraint arises where the electrons in the valence band can only be excited to the conduction band through the Dirac points. However, we find that, under this constraint, the excited electrons have no possibility to recombine with the hole. This differs from the situation of Ref. [35], where the laser field is applied along the Γ - K direction and the electron-hole recombination can occur for the electrons originating at the Dirac points.

To overcome this difficulty, we apply the stationary phase approximation only to three integral variables of \mathbf{K}_{0x} , \mathbf{K}_{0y} , t ,

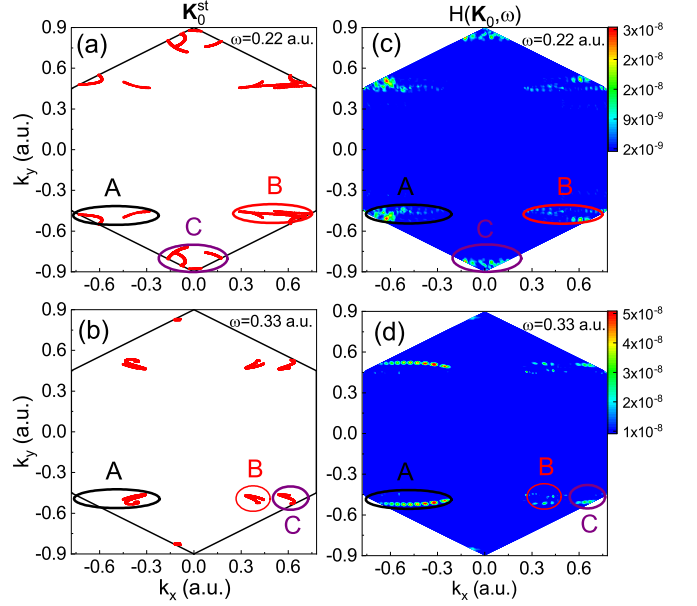


FIG. 2. For the harmonic frequency of $\omega = 0.22$ a.u. [(a) and (c)] and $\omega = 0.33$ a.u. [(b) and (d)], the red dots in (a) and (b) mark the saddle-point momenta \mathbf{K}_0^{st} calculated using Eqs. (2). The harmonic intensities $H(\mathbf{K}_0, \omega)$ calculated by TBDMEs are shown in (c) and (d). The different subpatterns marked by A, B, and C correspond to recombination times in the different half cycles of the short pulse as shown in Figs. 3(a) and 3(b). (For details, see Sec. IV of the Supplemental Material [37].)

and obtain following three saddle-point equations,

$$\int_{t'}^{t_r} \nabla_{\mathbf{K}_x^{\text{st}}(\tau)} \varepsilon_{cv}(\mathbf{K}_x^{\text{st}}(\tau), \mathbf{K}_{0y}^{\text{st}}) d\tau = 0, \quad (2a)$$

$$\int_{t'}^{t_r} \nabla_{\mathbf{K}_{0y}^{\text{st}}} \varepsilon_{cv}(\mathbf{K}_x^{\text{st}}(\tau), \mathbf{K}_{0y}^{\text{st}}) d\tau = 0, \quad (2b)$$

$$\varepsilon_{cv}(\mathbf{K}_x^{\text{st}}(t_r), \mathbf{K}_{0y}^{\text{st}}) - \omega = 0, \quad (2c)$$

in which t' and t_r represent the birth and recombination times of the electron-hole pair, respectively. $\mathbf{K}_0^{\text{st}} = (\mathbf{K}_{0x}^{\text{st}}, \mathbf{K}_{0y}^{\text{st}})$ is the saddle-point momentum and $\mathbf{K}_x^{\text{st}}(t) = \mathbf{K}_{0x}^{\text{st}} + A(t)$. Equations (2a) and (2b) represent the conditions for perfect electron-hole recombination trajectories [35], in contrast to imperfect recollisions [40–43]. The harmonic energy ω emitted during electron-hole pair recombination is given by Eq. (2c).

In practical numerical calculations, we choose initial momenta randomly distributed in the first BZ, and calculate the corresponding electron-hole trajectories that satisfy the three constraints in Eqs. (2). We illustrate the momenta of these saddle-point trajectories \mathbf{K}_0^{st} as red dots, corresponding to recombination energies of $\omega = 0.22$ and 0.33 a.u. in Figs. 2(a) and 2(b), respectively. Here, we consider the real-valued solutions of the five variables of t' , t_r , $\mathbf{K}_{0x}^{\text{st}}$, $\mathbf{K}_{0y}^{\text{st}}$, ω . Because of the three constraints in Eqs. (2), one can express ω as a function of $(\mathbf{K}_{0x}^{\text{st}}, \mathbf{K}_{0y}^{\text{st}})$. Therefore, for a selected frequency ω and the specific branch, the saddle-point trajectories form a 1D manifold in the momentum plane of $(\mathbf{K}_{0x}^{\text{st}}, \mathbf{K}_{0y}^{\text{st}})$.

In Figs. 2(c) and 2(d), we also present the harmonic intensities $H(\mathbf{K}_0, \omega)$ calculated by TBDMEs [37]. Upon comparing

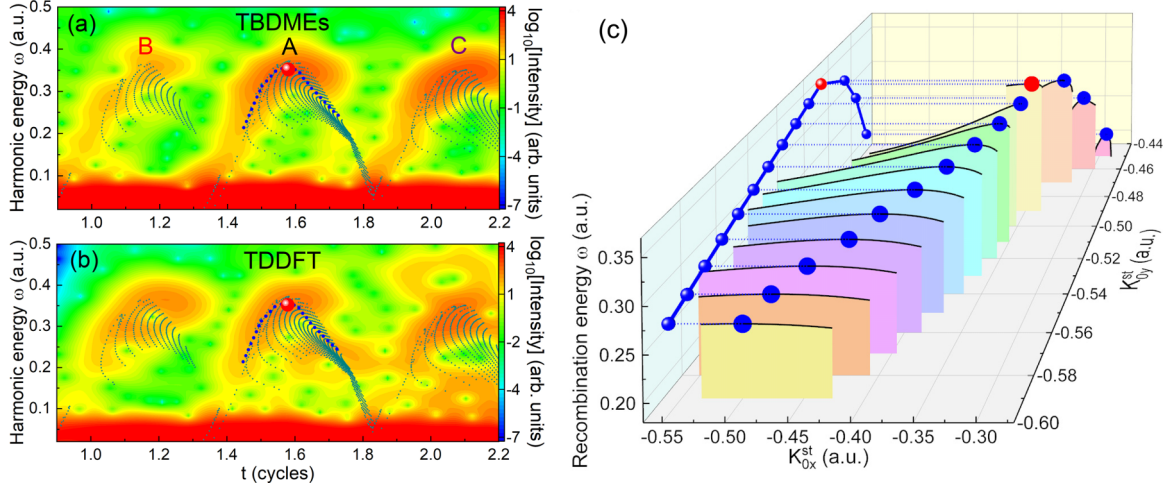


FIG. 3. (a), (b) The time-frequency distributions corresponding to the harmonic spectra shown in Fig. 1. In (a) and (b), the dark cyan points represent the recombination trajectories calculated by Eqs. (2). The subpatterns marked by A, B, and C correspond to the recombination times in the different half cycles of the short laser pulse. (c) The recombination energy ω as a function of the saddle-point momenta $\mathbf{K}_0^{st} = (K_{0x}^{st}, K_{0y}^{st})$ for branch A. The black curves show the relationship between the recombination energy ω and K_{0x}^{st} for specific K_{0y}^{st} . In (a)–(c), the blue dots indicate 1D caustic trajectories with $\partial\omega/\partial K_{0x}^{st} = 0$, and the red points ω^* indicate 2D caustic trajectories with $\partial\omega/\partial K_{0x}^{st} = \partial\omega/\partial K_{0y}^{st} = 0$ corresponding to branch A.

Fig. 2(a) with Fig. 2(c) and Fig. 2(b) with Fig. 2(d), one can see that the distribution of the saddle-point trajectories qualitatively aligns with the region where the harmonic intensities calculated by TBDMEs are relatively larger. This fact suggests that these perfect electron-hole recombination trajectories can cover the essential solutions.

Caustic effects on HHG. The harmonic intensity, denoted by $H(\omega)$, can be evaluated using $H(\omega) = \omega^2 |j(\omega)|^2$, where $j(\omega)$ from Eq. (1) can be deduced according to the saddle-point trajectories that satisfy Eqs. (2):

$$j(\omega) \sim \int_{-\infty}^{\infty} dt' \sum_{K_{0x}^{st}, K_{0y}^{st}, t_r} g(K_{0x}^{st}, K_{0y}^{st}, t_r, t') e^{-iS(K_{0x}^{st}, K_{0y}^{st}, t_r, t', \omega)} \times \frac{1}{\sqrt{|\det[S''(K_{0x}^{st}, K_{0y}^{st}, t_r, t', \omega)]|}} + \text{c.c.} \quad (3)$$

Here, $S''(K_{0x}^{st}, K_{0y}^{st}, t_r, t', \omega)$ is the Hessian matrix of the semiclassical action $S(K_{0x}^{st}, K_{0y}^{st}, t_r, t', \omega)$ with respect to K_{0x}^{st} , K_{0y}^{st} , and t_r , whose determinant is

$$\det[S''] = \frac{\partial\omega}{\partial K_{0x}^{st}} \mathcal{H}_1 - \frac{\partial\omega}{\partial K_{0y}^{st}} \mathcal{H}_2 - E(t_r) \frac{\partial\omega}{\partial K_{0x}^{st}} \mathcal{H}_3. \quad (4)$$

Here, \mathcal{H}_1 , \mathcal{H}_2 , and \mathcal{H}_3 are the second-order determinants (for the calculation details, refer to the Supplemental Material [37]).

We can then obtain the following caustic equations,

$$\partial\omega/\partial K_{0x}^{st} = 0, \quad \partial\omega/\partial K_{0y}^{st} = 0, \quad (5)$$

which determine a specific saddle-point trajectory that originates from the lattice momenta of $(K_{0x}^{st*}, K_{0y}^{st*})$ and finally emits a harmonic photon with energy ω^* . The caustic equations also imply that the multiple trajectories originating from the vicinity of $(K_{0x}^{st*}, K_{0y}^{st*})$ tend to emit harmonic photons with the same energy ω^* , demonstrating a kind of 2D caustic phenomenon. One can find the 2D caustic phenomenon is

caused by the two-dimensional nature of the reciprocal space plane of graphene and is closely related to the concrete form of the energy-band structure. According to Eqs. (3) and (4), we also find that, for this specific trajectory, the determinant of the Hessian matrix $S''(K_{0x}^{st*}, K_{0y}^{st*}, t_r^*, t'^*, \omega^*)$ becomes zero and the integrand diverges into infinity. According to our extensive numerical explorations, we find that the corresponding integral might be also divergent. This caustic singularity indicates a potentially significant amplification in the magnitude of the harmonics with the energy around ω^* .

Using the field parameters in Fig. 1 and with the help of saddle-point equations (2), we have solved the 2D caustic equations (5) and obtained $\omega^* = 0.35$ a.u., which is qualitatively in agreement with the location of the HES peak illustrated in Fig. 1. Notice the caustic singularity is different from the Van Hove singularities [14] of the energy bands that are determined by $|\nabla_{\mathbf{k}} \varepsilon_{cv}(\mathbf{k})| = 0$ and correspond to $\omega = 0.2$ and 0.6 a.u. as shown in Fig. 1. In our case, the excited electrons are accelerated along the Γ - M direction and the trajectories do not pass by the Van Hove singularities (see Fig. 2). In contrast, when the laser field is along the Γ - K direction as discussed in Ref. [35], the electron trajectories might pass by the Van Hove singularities. In this situation, the caustic singularities predicted by Eq. (5) could be consistent with the Van Hove singularities.

In Figs. 3(a) and 3(b), we present the time-frequency distributions corresponding to the harmonic spectra of Fig. 1 [37]. The results obtained from both TBDMEs and TDDFT demonstrate qualitative agreement. The red points correspond to the 2D caustic trajectory. One can find that the red point approximately locates at the brightest spot of the time-frequency distributions.

Corresponding to the recombination trajectories (the dark cyan points) shown in Figs. 3(a) and 3(b), we illustrate the recombination energy ω as a function of the saddle-point momenta $\mathbf{K}_0^{st} = (K_{0x}^{st}, K_{0y}^{st})$ in Fig. 3(c). In one-dimensional

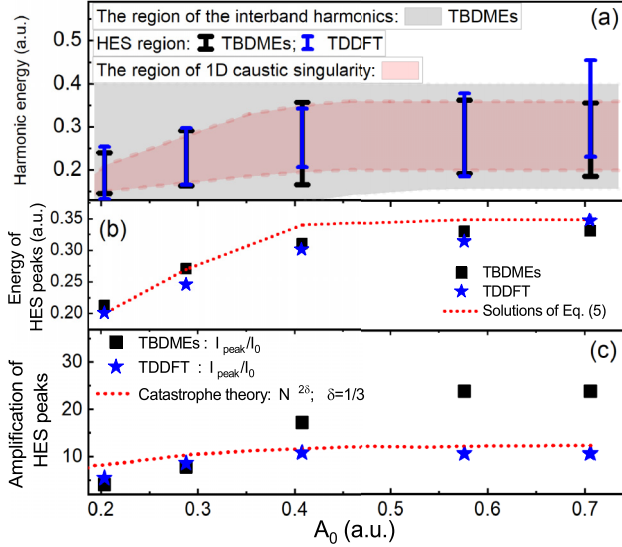


FIG. 4. (a) The gray area corresponds to the region where the interband currents dominate the harmonic generation according to TBDMEs (for details, see Sec. V of the Supplemental Material [37]). The HES regions are indicated by bars, which represent the energy intervals associated with the harmonic enhancement structure, corresponding to the energy regions of the blue dashed rectangles shown in Fig. 1. The pink area indicates the energy regions of 1D caustic singularities where $\partial\omega/\partial K_{0x}^{st} = 0$. (b) The black squares and blue stars show the energy of HES peaks as a function of A_0 , calculated by TBDMEs and TDDFT. At specific $A_0 = 0.58$ a.u., they correspond to local harmonic peaks denoted by the red arrows in Fig. 1. The red lines are the predictions of caustic equation (5). (c) The black square and blue star show the amplification of harmonic intensity at the HES peaks, calculated by I_{peak}/I_0 . The red line is the prediction of the catastrophe theory.

sections for a fixed K_{0y}^{st} , the blue dots indicate the local maxima of the recombination energies where $\partial\omega/\partial K_{0x}^{st} = 0$, termed as 1D caustic singularity. These trajectories are also marked by the blue dots in Figs. 3(a) and 3(b). Additional calculations reveal that for these trajectories, the determinant of $S''(K_{0x}^{st}, K_{0y}^{st}, t_r, t', \omega)$ is not zero but is relatively smaller, indicating a relatively higher-order harmonic enhancement due to the 1D caustic effect. It is noteworthy that the blue dots in Figs. 3(a) and 3(b) are approximately situated at the central area of the highlighted time-frequency distributions, suggesting that these particular trajectories may play a dominant role in the generation of interband harmonics [37].

Laser parameter-dependent caustic effects. We perform extensive calculations of HHG across a broad range of laser intensities. The HES information as a function of amplitude A_0 of the laser vector potential is shown in Fig. 4. Figure 4(a) shows that the energy regions of 1D caustic singularities are qualitatively consistent with those of HES simulated by both TBDMEs and TDDFT. In contrast to the atom situation where caustic effects are limited to a narrow regime around the cutoff energy of HHG [12,37], the caustics in graphene will lead to a broad energy region of HHG enhancement and even dominate the entire interband harmonic generation process.

Figure 4(b) clearly demonstrates that the energy of HES peaks can be approximately predicted by the caustic equation (5). It is seen that the peak energy tends to saturate to 0.35 a.u. with an increase of A_0 . This saturation energy is related to the maximum gap that the electron-hole pair can achieve during the excursion in the energy band. Note that the saturation of the cutoff frequency with the laser intensity is not related to the energy gap at the Γ point (i.e., 0.6 a.u.), because the electron-hole recombination trajectories do not pass by the Γ point (see Fig. 2).

The enhancement amplitude of the HES peaks can be roughly estimated by the catastrophe theory $I_{\text{peak}}/I_0 \approx N^{2\delta}$ [3,12]. Here, I_{peak} represents the intensity of the 2D caustic peak at ω^* . I_0 denotes the background harmonic intensity away from the caustic region. For specific $A_0 = 0.58$ a.u., they have been labeled in Fig. 1. N is the harmonic order corresponding to the caustic peak. The focusing index δ depends on the types of catastrophes, which are determined by the number of the control parameters and state variables. In the case of atoms excited by a linearly polarized monochromatic laser field, the harmonic amplitude can be evaluated by $E(\omega) = \int E_{XUV}(t_i, \omega) e^{-iS_0(t_i, \omega)} dt_i$ [12], in which $E_{XUV}(t_i, \omega)$ is the amplitude of the quantum trajectory associated with the ionization time t_i . In the semiclassical action $S_0(t_i, \omega)$, there is only one control parameter (ω) and one state variable (t_i), corresponding to the fold catastrophe with $\delta = 1/6$ [12].

In our case of graphene irradiated by a linearly polarized MIR laser field, according to the saddle-point equations (2), there are two state variables of K_{0x}^{st} , and K_{0y}^{st} . Then, the harmonic amplitude can be evaluated as $E(\omega) = \iint dK_{0x}^{st} dK_{0y}^{st} g(K_{0x}^{st}, K_{0y}^{st}, \omega) e^{-iS(K_{0x}^{st}, K_{0y}^{st}, \omega)}$. The types of catastrophes turn out to be elliptic umbilic or hyperbolic umbilic with the focusing index $\delta = 1/3$. If we assume that K_{0y}^{st} is fixed, the above 2D caustic singularity will degenerate to be a 1D caustic singularity corresponding to the fold catastrophe with focusing index $\delta = 1/6$, in analogy to atomic or 1D periodic potential cases [12,15].

Figure 4(c) indicates that catastrophe theory can roughly predict the tendency of the amplification of the HES peaks with increasing A_0 , while some deviations remain, especially for large A_0 . The TDDFT simulation includes multiple energy bands rather than the two energy bands of TBDMEs. Intuitively, one would expect that the catastrophe theory agrees better with the TBDMEs simulations than with the TDDFT simulations, while in our situation, the TDDFT results are closer to the prediction of the catastrophe theory. This might be an interesting issue for further study.

Summary. Our numerical simulations with both TBDMEs and TDDFT uncover a striking HES for the HHG in graphene, which we attribute to caustic effects. We have developed an electron-hole recombination trajectory theory and then deduced the caustic equations that can approximately predict the location of the HES peak as well as the width of HES. It is shown that catastrophe theory can roughly predict the tendency of the amplification of the HES peaks with increasing field strength. Our findings can be experimentally observed utilizing contemporary techniques [44], and our theoretical analysis is related to other 2D materials as well as bulk materials.

Acknowledgments. This work is supported by NSAF (Grant No. U2330401) and the National Natural Science Foundation

of China (Grant No. 11974057). We acknowledge valuable discussions with Dr. Jiaxiang Chen.

- [1] R. Thom, *Structural Stability and Morphogenesis: An Outline of a General Theory of Models* (Perseus Books, New York, 1989).
- [2] M. Berry and C. Upstill, *Catastrophe Optics: Morphologies of Caustics and Their Diffraction Patterns* (Elsevier, Amsterdam, 1980).
- [3] Y. A. Kravtsov and Y. I. Orlov, Caustics, catastrophes, and wave fields, *Sov. Phys. Usp.* **26**, 1038 (1983).
- [4] K. W. Ford and J. A. Wheeler, Semiclassical description of scattering, *Ann. Phys.* **7**, 259 (1959).
- [5] P. Sikivie, Caustic ring singularity, *Phys. Rev. D* **60**, 063501 (1999).
- [6] M. V. Berry, Nature's optics and our understanding of light, *Contemp. Phys.* **56**, 2 (2015).
- [7] Q. Z. Xia, J. F. Tao, J. Cai, L. B. Fu, and J. Liu, Quantum interference of glory rescattering in strong-field atomic ionization, *Phys. Rev. Lett.* **121**, 143201 (2018).
- [8] S. Brennecke, N. Eicke, and M. Lein, Gouy's phase anomaly in electron waves produced by strong-field ionization, *Phys. Rev. Lett.* **124**, 153202 (2020).
- [9] L. G. Liao, Q. Z. Xia, J. Cai, and J. Liu, Semiclassical trajectory perspective of glory rescattering in strong-field photoelectron holography, *Phys. Rev. A* **105**, 053115 (2022).
- [10] F. D. Tappert, *Wave Propagation and Underwater Acoustics* (Springer, Berlin, 1977).
- [11] T. A. Croft, HF radio focusing caused by the electron distribution between ionospheric layers, *J. Geophys. Res.* **72**, 2343 (1967).
- [12] O. Raz, O. Pedatzur, B. D. Bruner, and N. Dudovich, Spectral caustics in attosecond science, *Nat. Photon.* **6**, 170 (2012).
- [13] V. A. Birulia and V. V. Strelkov, Spectral caustic in two-color high-order harmonic generation: Role of Coulomb effects, *Phys. Rev. A* **99**, 043413 (2019).
- [14] A. J. Uzan, G. Orenstein, Á. Jiménez-Galán, C. McDonald, R. E. F. Silva, B. D. Bruner, N. D. Klimkin, V. Blanchet, T. Arusi-Parpar, M. Krüger, A. N. Rubtsov, O. Smirnova, M. Ivanov, B. Yan, T. Brabec, and N. Dudovich, Attosecond spectral singularities in solid-state high-harmonic generation, *Nat. Photon.* **14**, 183 (2020).
- [15] J. Chen, Q. Xia, and L. Fu, Spectral caustics of high-order harmonics in one-dimensional periodic crystals, *Opt. Lett.* **46**, 2248 (2021).
- [16] F. Krausz and M. Ivanov, Attosecond physics, *Rev. Mod. Phys.* **81**, 163 (2009).
- [17] X. F. Li, A. L'Huillier, M. Ferray, L. A. Lompre, and G. Mainfray, Multiple-harmonic generation in rare gases at high laser intensity, *Phys. Rev. A* **39**, 5751 (1989).
- [18] P. B. Corkum, Plasma perspective on strong field multiphoton ionization, *Phys. Rev. Lett.* **71**, 1994 (1993).
- [19] M. Lewenstein, Ph. Balcou, M. Yu. Ivanov, A. L'Huillier, and P. B. Corkum, Theory of high-harmonic generation by low-frequency laser fields, *Phys. Rev. A* **49**, 2117 (1994).
- [20] J. Itatani, J. Levesque, D. Zeidler, H. Niikura, H. Pépin, J. C. Kieffer, P. B. Corkum, and D. M. Villeneuve, Tomographic imaging of molecular orbitals, *Nature (London)* **432**, 867 (2004).
- [21] M. Meckel, D. Comtois, D. Zeidler, A. Staudte, D. Pavičić, H. C. Bandulet, H. Pépin, J. C. Kieffer, R. Dörner, D. M. Villeneuve, and P. B. Corkum, Laser-induced electron tunneling and diffraction, *Science* **320**, 1478 (2008).
- [22] C. Yu, S. Jiang, and R. Lu, High order harmonic generation in solids: a review on recent numerical methods, *Adv. Phys. X* **4**, 1562982 (2019).
- [23] S. Ghimire, A. D. DiChiara, E. Sistrunk, P. Agostini, L. F. DiMauro, and D. A. Reis, Observation of high-order harmonic generation in a bulk crystal, *Nat. Phys.* **7**, 138 (2011).
- [24] T. T. Luu, M. Garg, S. Yu. Kruchinin, A. Moulet, M. Th. Hassan, and E. Goulielmakis, Extreme ultraviolet high-harmonic spectroscopy of solids, *Nature (London)* **521**, 498 (2015).
- [25] G. Ndashimiye, S. Ghimire, M. X. Wu, D. A. Browne, K. J. Schafer, M. B. Gaarde, and D. A. Reis, Solid-state harmonics beyond the atomic limit, *Nature (London)* **534**, 520 (2016).
- [26] C. Yu, U. Saalman, and J. M. Rost, High-order harmonics from backscattering of delocalized electrons, *Phys. Rev. A* **105**, L041101 (2022).
- [27] H. Z. Liu, Y. L. Li, Y. S. You, S. Ghimire, T. F. Heinz, and D. A. Reis, High-harmonic generation from an atomically thin semiconductor, *Nat. Phys.* **13**, 262 (2017).
- [28] H. K. Keldar, U. Saalman, and J. M. Rost, Ultrashort laser-driven dynamics of massless Dirac electrons generating valley polarization in graphene, *Phys. Rev. Res.* **4**, L022014 (2022).
- [29] C. Heide, Y. Kobayashi, A. C. Johnson, T. F. Heinz, D. A. Reis, F. Liu, and S. Ghimire, High-harmonic generation from artificially stacked 2D crystals, *Nanophotonics* **12**, 255 (2023).
- [30] F. Dong, Q. Xia, and J. Liu, Ellipticity of the harmonic emission from graphene irradiated by a linearly polarized laser, *Phys. Rev. A* **104**, 033119 (2021).
- [31] F. Dong and J. Liu, Knee structure in the laser-intensity dependence of harmonic generation for graphene, *Phys. Rev. A* **106**, 043103 (2022).
- [32] D. Faccialà, S. Pabst, B. D. Bruner, A. G. Ciriolo, S. De Silvestri, M. Devetta, M. Negro, H. Soifer, S. Stagira, N. Dudovich, and C. Vozzi, Probe of multielectron dynamics in xenon by caustics in high-order harmonic generation, *Phys. Rev. Lett.* **117**, 093902 (2016).
- [33] H. K. Keldar, V. Apalkov, and M. I. Stockman, Graphene in ultrafast and superstrong laser fields, *Phys. Rev. B* **91**, 045439 (2015).
- [34] L. A. Chizhova, F. Libisch, and J. Burgdorfer, High-harmonic generation in graphene: Interband response and the harmonic cutoff, *Phys. Rev. B* **95**, 085436 (2017).
- [35] Ó. Zurrón, A. Picón, and L. Plaja, Theory of high-order harmonic generation for gapless graphene, *New J. Phys.* **20**, 053033 (2018).
- [36] H. K. Keldar, V. Apalkov, and M. I. Stockman, Wannier-Stark states of graphene in strong electric field, *Phys. Rev. B* **90**, 085313 (2014).

- [37] See Supplemental Material at <http://link.aps.org/supplemental/10.1103/PhysRevA.109.L041102> for details about graphene structure, numerical calculation methods, derivations of the Hessian matrix, and caustic effects on HHG in a model atom.
- [38] L. Keldysh, Ionization in the field of a strong electromagnetic wave, *Sov. Phys. JETP* **20**, 1307 (1965).
- [39] G. Vampa, C. R. McDonald, G. Orlando, D. D. Klug, P. B. Corkum, and T. Brabec, Theoretical analysis of high-harmonic generation in solids, *Phys. Rev. Lett.* **113**, 073901 (2014).
- [40] L. Yue and M. B. Gaarde, Imperfect recollisions in high-harmonic generation in solids, *Phys. Rev. Lett.* **124**, 153204 (2020).
- [41] A. M. Parks, G. Ernotte, A. Thorpe, C. R. McDonald, P. B. Corkum, M. Taucer, and T. Brabec, Wannier quasi-classical approach to high harmonic generation in semiconductors, *Optica* **7**, 1764 (2020).
- [42] Y. Feng, S. Shi, J. Li, Y. Ren, X. Zhang, J. Chen, and H. Du, Semiclassical analysis of ellipticity dependence of harmonic yield in graphene, *Phys. Rev. A* **104**, 043525 (2021).
- [43] R. Boyero-García, A. García-Cabrera, O. Zurrón-Cifuentes, C. Hernández-García, and L. Plaja, Nonclassical high harmonic generation in graphene driven by linearly polarized laser pulses, *Opt. Express* **30**, 15546 (2022).
- [44] N. Yoshikawa, T. Tamaya, and K. Tanaka, High-harmonic generation in graphene enhanced by elliptically polarized light excitation, *Science* **356**, 736 (2017).